Plasma Formation in Water by Picosecond and Nanosecond Nd:YAG Laser Pulses—Part I: Optical Breakdown at Threshold and Superthreshold Irradiance

Alfred Vogel, Kester Nahen, Dirk Theisen, and Joachim Noack

(Invited Paper)

***Abstract*— We investigated plasma formation in distilled water by 30-ps and 6-ns Nd : YAG laser pulses of 1064-nm and 532-nm wavelength for focusing angles between 1.7° and 32°. We determined the optical breakdown thresholds and analyzed the plasma length achieved at superthreshold irradiance. The parameter range investigated covers the parameters used for intraocular laser surgery. The experimental results are compared to theoretical models for the calculation of breakdown thresholds and the description of plasma growth for superthreshold breakdown. We found that at λ = 1064 nm the measured thresholds for both pulse durations coincide with the calculated thresholds for the generation of seed electrons by multiphoton ionization. The breakdown process is completed by avalanche ionization. The seed electron density required for breakdown is about 4×10^9 cm^{-3} for the 6-ns pulses, and 1.4×10^{11} cm^{-3} for the 30-ps pulses. No spot size dependence of the irradiance threshold for breakdown was observed. The average threshold is by a factor of 5.9 higher for 30-ps pulses ($I_{\mathrm{th}} = 4.5 \times 10^{11}$ W/cm^2) than for 6-ns pulses ($I_{\mathrm{th}} = 0.76 \times 10^{11}$ W/cm^2). At angles below approximately 2°, the threshold is influenced by self-focusing effects. The breakdown thresholds at 532 nm are slightly lower than at 1064 nm. Here, multiphoton ionization contributes considerably to the generation of free electrons throughout the whole process of plasma formation. Our results for plasma formation at superthreshold energies support a "breakdown wave" mechanism of plasma growth. For picosecond pulses, the breakdown threshold can be considered to be time-invariant, but for nanosecond pulses there is probably a decrease of the threshold during the laser pulse which may be due to UV-radiation emitted from plasma created at the beginning of the pulse. The plasma length $z_{\max}$ reached during the laser pulse depends strongly on the focusing angle, with this dependence being more pronounced for the picosecond pulses than for the nanosecond pulses. The dependence between plasma length and laser pulse energy can be expressed by $z_{\max} \propto (\beta - 1)^n$ with $\beta = E/E_{\mathrm{th}}$. We found $n = 0.54 \pm 0.02$ for 30-ps pulses, and $0.31 \leq n$ 0.47 for 6-ns pulses. At equal pulse energy E, nanosecond plasmas are always shorter than picosecond plasmas, whereas at equal normalized energy β nanosecond plasmas are always longer.**

Manuscript received September 16, 1996. This work was supported by the Deutsche Forschungsgemeinschaft, Grant Bi-321/2-3.

The authors are with the Medical Laser Center, Lübeck, Germany.

Publisher Item Identifier S 1077-260X(96)09598-6.

I. Introduction

In recent years, laser-induced plasma formation has been used in various fields of laser medicine for photodisruption, ablation, or lithotripsy [1], [2], and it has become especially important in intraocular microsurgery [3], [4]. This has raised an interest in gaining a better understanding of plasma formation in liquids which for many years received less attention than plasma formation in solids and gases [5]–[8]. To achieve precise and well-localized tissue effects, it is important to know how the threshold for plasma formation (optical breakdown threshold) depends on the laser pulse duration and the focusing geometry, and how these parameters influence the plasma length achieved at superthreshold pulse energies. Both questions are the topics of the present study. Breakdown thresholds and plasma length are experimentally investigated, and the results are compared to theoretical models developed by Kennedy [9] and Docchio *et al.* [10]. Besides giving guidelines for surgical laser applications, an investigation of the laws governing the plasma length can also give insight into the physical mechanism of plasma growth at super-threshold irradiance.

The focusing angles investigated in this study are between 1.7° and 32° $(1/e^2)$, i.e., they cover the range of focusing angles clinically applied. This is in contrast to the earlier work done by Doccio *et al.* [11] and Sacchi [12] who investigated breakdown thresholds for very small focusing angles between 0.22° and 1.7°. We took great care to realize well-defined experimental conditions allowing a comparison of the measurement results with predictions of theoretical models. Aberrations of the optical delivery system were minimized and the actual spot size was measured, in contrast to earlier work by Loertscher [13], Docchio *et al.* [11], Zysset *et al.* [14], and Vogel *et al.* [15] who assumed diffraction limited spot sizes. For the first time, the plasma length was investigated for a wide range of laser parameters. For small focusing angles, special attention was paid to the influence of self-focusing on the breakdown threshold. Self-focusing was detected by observing the occurrence of plasma filaments [16] and continuum generation [17]. To elucidate the wavelength dependence of the

breakdown process, we compared the breakdown thresholds at 1064 nm and 532 nm. Most investigations were, however, done at a wavelength of $\lambda = 1064$ nm, because this wavelength is optimally suited for intraocular surgery due to the high transmission of the ocular media, the low absorption at the retina, and the invisibility of the radiation avoiding dazzling of the patient. The pulse durations investigated were 6 ns and 30 ps. The present study is complemented by investigations of the transmission, scattering and reflection of laser light by the plasma presented in a related paper [18].

II. Theoretical Background

A. Breakdown Thresholds

At an irradiance above approximately 10^{10} W/cm^2, plasma formation occurs even in nominally transparent media like distilled water or the ocular media [11], [19]. There are two mechanisms which can lead to plasma formation: direct ionization of the medium by multiphoton absorption or avalanche ionization via inverse bremsstrahlung absorption [20], [21]. The ionization process is called "optical breakdown" when a critical free electron density $\rho_{\rm cr} \approx 10^{18}$ cm^{-3} is exceeded during the laser pulse [5], [22]. For water, this electron density corresponds to a fractional ionization of about 1.5×10^{-5} [9], [22].

Avalanche ionization requires a few free electrons to be present in the focal volume at the beginning of the laser pulse. These "seed electrons" for the ionization cascade can be generated either by heating of linearly absorbing impurities in the liquid or by multiphoton ionization. In pure media, multiphoton ionization is the only mechanisms which can provide seed electrons. The multiphoton ionization rate is proportional to I^k, where I is the intensity of the beam, and k is the number of photons required for ionization [8]. The value of the proportionality constant decreases with increasing k, i.e., with increasing wavelength where more photons are needed to provide the energy necessary for ionization. At $\lambda = 1064$ nm, 11 photons are required to ionize single water molecules having an ionization energy of 12.6 eV, and the probability for multiphoton ionization is therefore very small. Recently, Sacchi [12] argued that one should not consider the ionization energy of single molecules, but treat liquid water as an amorphous semiconductor [23] and look at the energy required for the excitation of electrons from the $1b_1$ molecular orbital to an exciton band (6.5 eV [24]). This approach yields a lower value of k ($k = 6$ for $\lambda = 1064$ nm), and thus a higher probability for multiphoton processes than formerly assumed. It has been supported by the results of Kennedy *et al.* [25], and will therefore be followed also in the present study.

With decreasing pulse duration, the irradiance I must increase for the critical electron density to be reached during the shorter pulse duration. The cascade ionization rate $\eta_{\rm casc}$ is proportional to the irradiance I when electron losses are neglected: $\eta_{\rm casc} \propto I$ [26]. Since the multiphoton ionization rate has the much stronger irradiance dependence $\eta_{mp} \propto I^k$, multiphoton processes become ever more important with decreasing pulse duration. Kennedy [9] pointed out that the details of the interplay between cascade and multiphoton processes depend on the ratio of the threshold I_c for the completion of the ionization cascade during the laser pulse and the threshold I_m for the creation of an initial electron density ρ_0 by multiphoton ionization.

He discussed three possible scenarios.

"Long" Pulses— $I_c < I_m$: Cascade ionization is the dominating mechanism. In pure media, however, multiphoton ionization is needed for the creation of initial electrons, and the measured threshold $I_{\rm th}$ coincides with I_m.

"Short" Pulses— $I_c > I_m$: Multiphoton ionization contributes considerably to the creation of free electrons throughout the whole process of plasma formation. The measured threshold is an intermediate value between I_c and I_m.

"Ultrashort" Pulses— $I_c \gg I_m$: Multiphoton ionization is the dominating mechanism, because at the high irradiance values required for breakdown the multiphoton ionization rate is much higher than the cascade ionization rate. The measured threshold is given by the irradiance I_{MP} rendering the critical electron density $\rho_{\rm cr}$ at the end of the laser pulse.

Based on the work of Keldysh [27], Kennedy obtained for I_m [9]

$$I_m = \frac{2}{B}\left(\frac{\rho_{0\,\min}}{\Delta t A}\right)^{1/k}. \tag{1}$$

Here, A and B are constants which depend on the breakdown medium and the laser wavelength ($A = 1.3908 \times 10^{40}$ s$^{-1}\cdot$ m^{-3}, $B = 4.9231 \times 10^{-18}$ m$^2\cdot$ W^{-1} for water and $\lambda = 1064$ nm, and $A = 7.305 \times 10^{41}$ s$^{-1}\cdot$ m^{-3}, $B = 1.231 \times 10^{-18}$ m$^2\cdot$ W^{-1} for $\lambda = 532$ nm). $\rho_{0\,\min}$ is the minimal initial density of free electrons required to start an ionization cascade that leads to $\rho_{\rm cr}$ at the end of the pulse, and Δt is the time required for the generation of $\rho_{0\,\min}$.

An extension of Shen's theory of avalanche ionization [26] led to an expression for I_c [9]

$$I_c = \left(\frac{mcn_0\varepsilon_0 E_{\rm ion}}{e^2}\,\frac{1+4\pi^2\nu^2\tau^2}{\tau}\right)\left[g + \frac{2}{t_L}\ln\left(\frac{\rho_{\rm cr}}{\rho_0}\right)\right] + \frac{m^2 E_{\rm ion} 4\pi^2\nu^2 c n_0\varepsilon_0}{e^2 M}. \tag{2}$$

The three terms in (2) represent, in order, diffusion losses, carrier buildup through cascade ionization, and collisional energy losses. $E_{\rm ion} = 6.5$ eV is the energy required for an electron to transit from the $1b_1$ molecular orbital to an exciton band, m and e are the electron mass and charge, respectively, ρ_0 is the initial electron density provided by multiphoton ionization, τ is the mean free time between inelastic collisions between electrons and heavy particles, M is the mass of a water molecule, t_L is the laser pulse duration, ν is the frequency of the laser light, n_0 is the index of refraction of the medium at frequency ν, ε_0 is the permittivity of free space, c is the vacuum velocity of light, and g is the rate of electron losses due to recombination, trapping in solvated states, and diffusion out of the focal volume of the beam. The losses are small in condensed media for pulses of 10^{-8} s or less and at fields close to the breakdown threshold [9].

The threshold I_{MP} for pure multiphoton ionization is given by [9]

$$I_{MP} = \frac{1}{B}\left(\frac{\rho_{\mathrm{cr}}}{A\Delta t'}\right)^{1/k} \tag{3}$$

where $\Delta t'$ is the time required to reach the critical electron density ρ_{cr}.

For the calculation of the actual breakdown thresholds, Kennedy [9] somewhat arbitrarily assumed a constant number $N_{0\,\mathrm{min}}$ of initial electrons ($N_{0\,\mathrm{min}} = 1$ for nanosecond pulses, $N_{0\,\mathrm{min}} = 10$ for picosecond-pulses), and deduced $\rho_{0\,\mathrm{min}}$ from $N_{0\,\mathrm{min}}$ through $\rho_{0\,\mathrm{min}} = N_{0\,\mathrm{min}}/V_f$, where V_f is the focal volume. It is approximated by a cylinder with diameter $2\omega_o$ and length $z_0 = \pi\omega_0^2/\lambda$. Kennedy assumed a time $\Delta t = t_L/10$ for the generation of the initial electrons by multiphoton ionization, and a time $\Delta t' = t_L/2$ for the ionization cascade. A critical density $\rho_{\mathrm{cr}} = 10^{20}/\mathrm{cm}^3$ was used as breakdown criterion for pulse durations >10 ps. Other constants used were $M = 3 \times 10^{-26}$ kg for the mass of a water molecule, $n_0 = 1.32$ for the index of refraction of water, and $\tau = 10^{-15}$ s for the mean free time between inelastic collisions between electrons and heavy particles.

Our experimental investigations allow to compare measured thresholds I_{th} at various focusing angles and pulse durations with the calculated thresholds I_m and I_c. This will add to the physical understanding of the respective breakdown mechanisms, and create a data base for an estimation of $N_{0\,\mathrm{min}}$ and $\rho_{0\,\mathrm{min}}$ for a broad range of experimental conditions.

B. Optical Breakdown at Superthreshold Irradiance

Plasma-mediated laser surgery is always performed at superthreshold irradiance, i.e., under conditions where plasma formation starts at the laser focus and the plasma expands toward the incoming laser beam during the laser pulse [10]. The plasma expansion is thereby largely restricted to the side proximal to the laser because of the light absorption within the plasma ("plasma shielding"). An understanding of the mechanisms and laws governing the plasma growth and the final plasma length is essential for an optimal control of the surgical procedure.

The plasma growth in gases has been interpreted as a radiation-supported detonation wave [28], [29]. A shock wave is emitted from the point where plasma is formed first. The medium is thereby compressed and partly ionized at the shock front. The free electrons lead to an increase in light absorption and thus to plasma formation. The propagation of the plasma front in turn drives the shock front. This model can be valid in gases where high shock wave velocities and high temperatures at the shock front are reached [20], but is not applicable to liquids, as shown by the following example. After a 10-mJ Nd : YAG laser pulse of 6-ns duration, the shock pressure at the plasma rim is about 7000 MPa [30]. This corresponds to a temperature rise at the shock front of about 350 K [31] which is by far too low to result in any appreciable ionization. Furthermore, the initial shock wave velocity is only 4.5 km/s [30] and thus too small to explain average plasma front velocities between 12 km/s and 76 000 km/s which are observed in this study. An alternative explanation of plasma growth is the moving breakdown model which was developed by Ambartsumyan *et al.* [32] and Raizer [20], and later refined by Docchio *et al.* [10]. It assumes that the breakdown occurs independently at each location on the optical axis as soon as the irradiance of the electric field surpasses the threshold value. It can account for the high plasma front velocities observed experimentally and is therefore taken as a basis for the interpretation of our experimental data.

The moving breakdown model relies on some simplifying assumptions: 1) the time required for breakdown to occur is negligible; 2) the breakdown threshold is independent of the beam diameter; and 3) the threshold is constant in time, i.e., plasma formed early during the laser pulse does not influence the breakdown threshold in the vicinity of the plasma. For a laser pulse with Gaussian shape and beam profile, Docchio derived the following relation between the plasma length z_{max} reached at maximum irradiance of the laser pulse and the normalized laser pulse energy $\beta = E/E_{\mathrm{th}} = I/I_{\mathrm{th}}$ [10]

$$z_{\mathrm{max}} = z_R\sqrt{\beta - 1}. \tag{4}$$

Here $z_R = \pi\omega_0^2/\lambda$ is the Rayleigh range and ω_0 the radius of the focal spot. The dependence between z_{max} and focusing angle θ is given by

$$z_{\mathrm{max}} = \frac{\lambda}{\pi\ \tan^2\dfrac{\theta}{2}}\ \sqrt{\beta - 1}. \tag{5}$$

The dependence of the plasma length on laser pulse duration is only implicitly contained in (4) and (5), and its evaluation requires knowledge of the breakdown threshold E_{th} at the pulse durations of interest. E_{th} determines the value of β for each laser pulse energy and duration, and this in turn allows to calculate z_{max}.

In this study, the predictions and assumptions of the moving breakdown model are examined by measurements of the plasma length at a variety of pulse energies, durations, and focusing angles.

III. Experimental Methods

1) Plasma Generation: The experimental arrangement for the investigation of plasma formation is depicted in Fig. 1. We used a Nd : YAG laser system (Continuum YG 671-10) emitting either nanosecond pulses (6 ns) or picosecond pulses (30 ps) at wavelengths of 1064 nm or 532 nm. The beam profile of the picosecond pulses was Gaussian (TEM_{00}), and the pulse-to-pulse fluctuations of the energy were in the range of $\pm$10%. The nanosecond pulses were generated in an instable resonator with variable reflectivity mirrors [33] providing a nearly Gaussian intensity profile modulated by a weak ring structure [Fig. 2(a)]. The pulse-to-pulse stability of the energy was better than $\pm$2%. The temporal shape of the nanosecond pulses exhibited some fluctuations; the average pulse form is shown in Fig. 2(c). At 532 nm, the pulse duration was 6% shorter than at 1064 nm, but both pulses will be referred to as "6-ns pulses" to facilitate the description of our results. The energy was varied without changing the beam profile by means of a rotatable half wave plate between two polarizers [15].

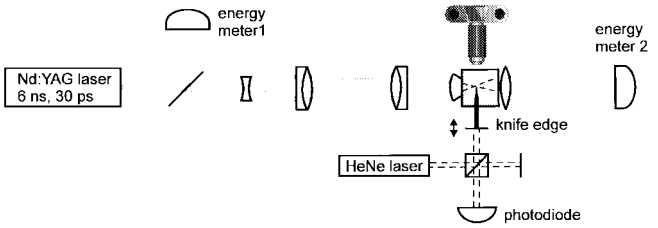

Fig. 1. Experimental arrangement for the investigation of plasma formation.

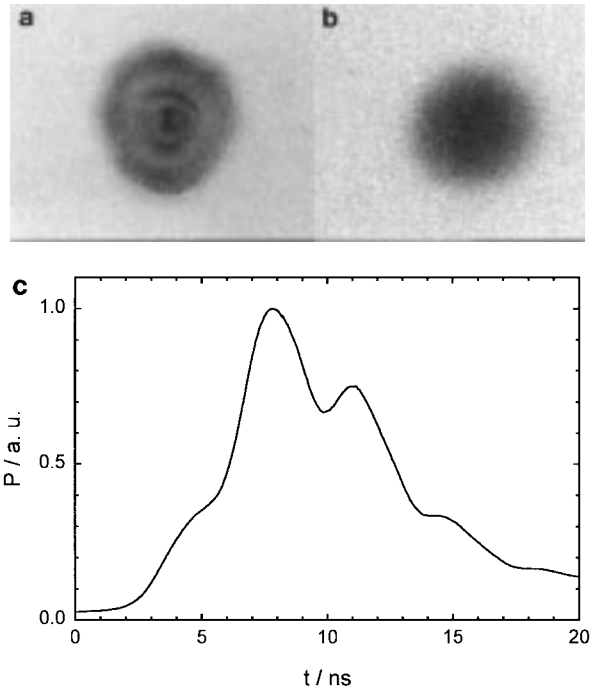

Fig. 2. Burn patterns of (a) a 6 ns pulse, (b) a 30-ps pulse, and (c) pulse form of the 6-ns pulse, averaged over 500 pulses.

The laser pulses were focused into a glass cuvette filled with distilled water. We investigated focusing angles between 1.8° and 32° for nanosecond pulses, and between 1.7° and 28° for picosecond pulses. The laser beam was expanded to allow large focusing angles together with a large distance between focus and cuvette walls. In this way, damage of the cuvette could be avoided even at high laser pulse energies. To minimize spherical aberrations, Nd : YAG laser achromats were used for the beam collimation and focusing ($f = 120$ mm), and an ophthalmic contact lens (Rodenstock RYM) was built into the cuvette wall. The laser focus coincided with the aplanatic point of the contact lens. Different focusing angles were realized by varying the beam expansion before focusing. The upper limit for the beam expansion is given by the requirement that vignetting of the laser beam by the lens mounts must be avoided to ensure a constant beam profile. The largest focusing angles at each pulse duration were therefore realized by adding an aplanatic meniscus lens between the focusing achromat and the contact lens. For the smallest focusing angles the beam expansion was removed.

During each laser exposure, the pulse energy was measured using a pyroelectric energy-meter (Laser Precision Rj 7100). Before the measurements, the energy-meter had been calibrated against a second instrument directly in front of the glass cuvette. To obtain the energy incident into the laser focus, the measured energy values were corrected for the absorption occurring in the water between contact lens and focus ($\alpha = 0.13$ cm^{-1}).

We used distilled water as a model for the intraocular fluids to provide reproducible experimental conditions. This is justified by the fact that the threshold for plasma formation in distilled water and the ocular media are similar [19], [34]. The water was further purified using a 0.22-μm filter (Millipore Sterifil-D-GS).

2) Determination of Focusing Angle and Spot Size: To determine the focusing angle θ, the diameter of the parallel beam was measured in front of the focusing lens, and the further beam propagation followed by means of a ray tracing program. The beam diameter was obtained by measuring the transmission through an aperture which was reduced stepwise in size. Assuming a Gaussian intensity profile, the transmission is [35]

$$T = 1 - e^{-2(r_a/\omega)^2} \tag{6}$$

where r_a is the radius of the aperture, and ω is the beam radius at the $1/e^2$ irradiance values. To determine ω, the function (6) was fitted to the measured $T(r_a)$ data using ω as a fit parameter.

The spot size was determined using a knife edge technique [36]. The knife edge was moved by a piezoelectric translation device and its position monitored by means of a Michelson interferometer (Fig. 1). The laser pulse energy used for the spot size measurement was kept small enough to avoid plasma formation at the knife edge. The beam radius was determined in various planes in the region of the beam waist. The beam propagation in this region is given by [37]

$$\omega(z) = \omega_0 \sqrt{1 + \left(\frac{M^2 \lambda z}{\pi \omega_0^2}\right)^2} \tag{7}$$

where $2\omega_0$ is the spot diameter, $\omega(z)$ is the beam radius at location z along the optical axis, and M is a parameter describing the "quality" of the beam. Equation (7) was fitted to the measurement data for $\omega(z)$ in order to obtain ω_0.

3) Determination of Breakdown Threshold: The breakdown thresholds were determined by counting how frequently plasma formation occurred as the energy was varied from subthreshold to superthreshold values. For each energy value, 20–50 laser exposures were evaluated. The pulses were released in time intervals of 30 s to avoid plasma initiation at the gas bubbles which remain for a few seconds in the vicinity of the laser focus after each laser pulse. Occurrence of breakdown was visually detected in a darkened room by observation of the plasma radiation. To determine the energy value E_{th} for 50% breakdown probability, the breakdown probability W was plotted as a function of the incident energy E_{in}, and the Gaussian error function was fitted to the measured data. We also determined the "sharpness" of the threshold which we define by $S = E_{\mathrm{th}}/\Delta E$ (see Fig. 3). ΔE is the energy interval between 10% and 90% breakdown probability.

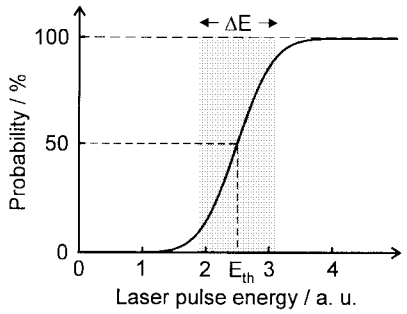

Fig. 3. Definition of the "sharpness" $S = E_{\rm th}/\Delta E$ of the breakdown threshold. ΔE is the energy interval between 10% and 90% breakdown probability.

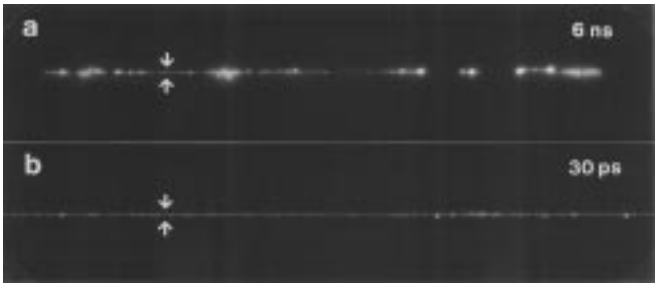

Fig. 4. Filament formation at small focusing angles: (a) 6-ns pulse duration, 1.8° focusing angle. (b) 30-ps pulse duration, 1.7° focusing angle. The diameter of the beam waist measured at low laser power is indicated by arrows.

4) Plasma Photography and Determination of Plasma Length: The plasma form and length were investigated by taking photographs with 7× magnification using a Leitz Photar lens $(F = 3.5)$ which provided a spatial resolution of about 4 μm. Depending on the brightness of the plasma radiation, we used Kodak T Max 400 film (for picosecond plasmas), Kodak T Max 100, or Agfapan APX 25 film (for nanosecond plasmas). To mark the location of the beam waist on the plasma photographs, a needle tip was adjusted above the location where a plasma is produced at threshold. The plasma length $z_{\rm max}$ extending from the beam waist toward the laser was measured from the photographic negatives using a microscope. To detect self-focusing effects, we inspected the plasma photographs for signs of filament formation. Continuum radiation which is also indicative for self-focusing effects [17] was observed on a white screen behind the water-filled cuvette and photographically recorded using the body of a 35-mm camera placed behind the cuvette.

IV. Results and Discussion

A. Breakdown Thresholds

1) Spot Size and Threshold Values: The measured values for spot size and energy threshold $E_{\rm th}$, as well as the corresponding values for the irradiance threshold $I_{\rm th}$, the radiant exposure threshold $F_{\rm th}$, and the power threshold $P_{\rm th}$ are listed in Tables I and II. For comparison, the diffraction limited spot sizes and the corresponding values of $I_{\rm th}$ and $F_{\rm th}$ are also given. At small focusing angles, the measured and diffraction limited spot size are almost identical, but at large angles, where aberrations are more difficult to control, the measured and diffraction limited spot size deviate by a factor of up to 2.3 for nanosecond pulses and 1.7 for picosecond pulses. The deviation is smaller with picosecond pulses because of their clean Gaussian beam profile. The parameter dependence of the threshold values is discussed below, after analyzing the role of self-focusing which may influence the spot size dependence of the breakdown thresholds.

2) Self-Focusing and Continuum Generation: For self-focusing to occur, a critical power $P_{\rm cr}$ has to be surpassed, regardless of the spot size. For optical breakdown, however, a certain irradiance must be exceeded. With increasing spot size (i.e., decreasing focusing angle) the laser power must be increased to reach the irradiance threshold. Below a certain focusing angle, the power required for optical breakdown will thus be higher than the critical power $P_{\rm cr}$ for self focusing, and at even smaller angles, it will exceed the critical value $P'_{\rm cr}$ for beam collapse and filament formation. We observed filament-like plasmas at $\theta = 1.8°$ for the 6-ns pulses, and at $\theta = 1.7°$ for the 30-ps pulses, as shown in Fig. 4. At these focusing angles plasma formation was always accompanied by self-focusing, even at the breakdown threshold. The diameter of the filaments is about 5 μm, as compared to a measured focus diameter of 48 μm. The filaments produced by the 30-ps pulses are homogeneously thin, whereas the filaments from the 6-ns pulses are interspersed by thicker plasma spots having a diameter of up to about 45 μm. With picosecond pulses, filament formation was also observed at larger focusing angles (4° and 8.5°), but only at energies far above the breakdown threshold [see Fig 6(b)].

The theoretical threshold for filament formation with Gaussian beams is $P'_{\rm cr} = 3.77c\lambda^2/32\pi^2 n_2$, where n_2 is the value of the nonlinear refractive index [5], [38]. With $n_2 = 1.7 \pm 0.85 \times 10^{-13}$ esu for water at 1064 nm [17], we obtain $P'_{\rm cr} = 2.38 \pm 1.2$ MW. This value is below the laser power at breakdown threshold for 30-ps pulses ($P_{\rm th} = 5.9$ MW at $\theta = 1.7°$), and slightly above the threshold value for nanosecond pulses ($P_{\rm th} = 1.34$ MW at $\theta = 1.8°$ which is still within the error margins of $P'_{\rm cr}$). Our finding that self-focusing influences nanosecond- and picosecond optical breakdown at small focusing angles is in agreement with the results of Soileau *et al.* for laser-induced damage in solids [39].

The reduction of the beam diameter by self-focusing increases the irradiance and thus the likelihood of plasma formation. The values for $I_{\rm th}$ given in Tables I and II refer, however, to the spot size measured at low intensities and are therefore lower estimates for the actual irradiance at which breakdown has occurred. A reduction of the beam diameter starts already at laser powers smaller than the threshold for filament formation. The actual threshold irradiance I_{SF} corresponding to the reduced beam diameter is, according to Soileau *et al.* [39], for $P \leq P'_{\rm cr}/4$ approximately given by

$$I_{SF} = \frac{I_{\rm th}}{1 - P/P'_{\rm cr}}. \tag{8}$$

The I_{SF} values calculated from our measurements are summarized in Table III. No values are given in cases where $P > P'_{\rm cr}/4$.

TABLE I
SPOT SIZE AND BREAKDOWN THRESHOLDS AT 6-ns PULSE DURATION

$\frac{\lambda}{\text{nm}}$	$\frac{\Theta}{^\circ}$	$\frac{E_{th}}{\mu\text{J}}$	$\frac{P_{th}}{\text{kW}}$	S	diffraction limited			measured		
					$\frac{2\omega_0}{\mu\text{m}}$	$\frac{F_{th}}{\text{Jcm}^{-2}}$	$\frac{I_{th}}{10^{11}\text{Wcm}^{-2}}$	$\frac{2\omega_0}{\mu\text{m}}$	$\frac{F_{th}}{\text{Jcm}^{-2}}$	$\frac{I_{th}}{10^{11}\text{Wcm}^{-2}}$
1064	32.0	89.9±0.8	15.0±0.1	2.47	2.36	2055±34	3.42±0.05	5.39±0.60	394±87	0.66±0.15
1064	22.0	140.6±1.3	23.4±0.3	2.05	3.48	1477±14	2.46±0.02	7.66±0.31	305±25	0.51±0.04
1064	8.0	493.4±11.3	82.2±1.8	2.06	9.69	669±15	1.12±0.03	11.53±0.42	472±36	0.79±0.06
1064	5.4	1082.0±22.0	180.3±3.7	2.16	14.36	668±14	1.11±0.02	14.57±0.60	648±54	1.08±0.09
1064	1.8	8022.9±283.8	1337.2±47.3	0.90	45.66	489±19	0.82±0.02	47.78±1.14	447±47	0.75±0.08
			mean:	1.93				mean:	453	0.76
532	22.0	38.5±0.6	6.4±0.1	1.51	1.74	1615±24	2.69±0.04	5.31±0.23	174±15	0.29±0.03

TABLE II
SPOT SIZE AND BREAKDOWN THRESHOLDS AT 30-ps PULSE DURATION

$\frac{\lambda}{\text{nm}}$	$\frac{\Theta}{^\circ}$	$\frac{E_{th}}{\mu\text{J}}$	$\frac{P_{th}}{\text{kW}}$	S	diffraction limited			measured		
					$\frac{2\omega_0}{\mu\text{m}}$	$\frac{F_{th}}{\text{Jcm}^{-2}}$	$\frac{I_{th}}{10^{11}\text{Wcm}^{-2}}$	$\frac{2\omega_0}{\mu\text{m}}$	$\frac{F_{th}}{\text{Jcm}^{-2}}$	$\frac{I_{th}}{10^{11}\text{Wcm}^{-2}}$
1064	28.0	2.30±0.01	76.7±0.3	2.93	2.72	39.59±0.17	13.20±0.06	4.60±0.48	13.84±2.89	4.61±0.96
1064	22.0	2.38±0.01	79.3±0.3	4.94	3.48	25.02±0.11	8.34±0.04	4.72±0.38	13.60±2.19	4.53±0.73
1064	14.0	5.00±0.07	166.7±2.3	3.24	5.51	20.97±0.29	6.99±0.10	5.80±0.34	18.92±2.23	6.31±0.74
1064	8.5	9.85±0.15	328.3±5.0	3.60	9.11	15.11±0.23	5.04±0.08	9.60±0.42	13.60±1.21	4.53±0.40
1064	4.0	33.29±0.39	1109.7±13.0	2.85	19.39	11.27±0.13	3.76±0.04	19.54±0.36	11.10±0.43	3.70±0.14
1064	1.7	178.54±2.62	5951.3±87.3	3.75	45.66	10.90±0.16	3.32±0.05	47.74±3.12	9.97±1.31	3.32±0.44
			mean:	3.55				mean:	13.5	4.5
532	22.0	1.01±0.001	33.7±0.02	4.21	1.74	42.38±0.20	14.13±0.07	3.38±0.32	11.25±2.17	3.75±0.72

TABLE III
THRESHOLDS I_{SF} FOR OPTICAL BREAKDOWN AT 1064 nm CALCULATED FROM I_{th} FOR $P < P'_{\text{cr}}/4$ USING (8)

6 ns				30 ps			
$\frac{\Theta}{^\circ}$	$\frac{P_{th}}{\text{MW}}$	$(1-\frac{P_{th}}{P'_{cr}})^{-1}$	$\frac{I_{th}^{SF}}{10^{11}\text{Wcm}^{-2}}$	$\frac{\Theta}{^\circ}$	$\frac{P_{th}}{\text{MW}}$	$(1-\frac{P_{th}}{P'_{cr}})^{-1}$	$\frac{I_{th}^{SF}}{10^{11}\text{Wcm}^{-2}}$
32.0	0.015	1.006	0.66	28.0	0.076	1.033	4.76
22.0	0.023	1.010	0.51	22.0	0.079	1.034	4.69
8.0	0.082	1.036	0.82	14.0	0.167	1.075	6.78
5.4	0.180	1.082	1.17	8.5	0.328	1.160	5.25
1.8	1.337			4.0	1.110		
				1.7	5.951		

With 30-ps pulses and a focusing angle of 1.7°, we observed continuum generation in the visible range of the spectrum. The threshold for 50% probability of continuum generation was five times the breakdown threshold ($E_{\text{cont}} = 1.02 \pm 0.02$ mJ, $P_{\text{cont}} = 33.9 \pm 0.6$ MW). The patterns created by the continuum radiation on a screen behind the cuvette were similar to those described previously by Smith *et al.* [17]. At 4° focusing angle, continuum generation was sometimes also observed, but only at pulse energies above 2.5 mJ.

It is remarkable that Docchio *et al.* [11] did not report self-focusing or continuum generation, although they used very small focusing angles of 0.2°–1.7° (these values are deduced from the focal areas given in [11]). One reason may be that they observed the plasmas with the naked eye, but did not photograph the plasma radiation. In our study, self-focusing was revealed only by analysis of the plasma photographs.

3) Threshold Dependence on Spot Size: We observed no systematic dependence between breakdown threshold and spot size (Tables I–III). In particular, the threshold values did not increase for smaller spot sizes as would be expected if losses by electron diffusion out of the focal volume played a major role. The lack of a spot size dependence justifies the assumption made in the moving breakdown model (Section II-B) that the threshold is independent of the laser beam diameter.

Our findings are in contrast to the work of Loertscher [13] and Docchio *et al.* [11] who state that the breakdown threshold increases with decreasing spot size. They interpret this as a consequence of electron diffusion out of the focal volume of the laser beam. Loertscher investigated large focusing angles between 8° and 16° where it is hard to completely eliminate optical aberrations. Nevertheless, he did not measure the actual spot size, but calculated I_{th} assuming diffraction limited conditions. As already pointed out by Evans and Morgan [41], and as demonstrated by the data in Tables I and II, this can lead to an apparent spot size dependence of I_{th}, because aberrations usually become more pronounced with larger focusing angles.

Docchio investigated very small focusing angles $\leq 1.7°$ at which, according to our results, the breakdown process is influenced by self-focusing of the laser beam. The spot size

dependence reported by him is much stronger for picosecond pulses than for nanosecond pulses. Hence, it cannot be due to electron diffusion out of the focal volume which is negligible for picosecond pulses. We believe that it is rather an artefact related to self-focusing: The decrease of the beam diameter resulting from self-focusing leads to a lowering of the energy threshold for breakdown, and, if $I_{\rm th}$ is calculated assuming diffraction limited conditions, to an apparent decrease of $I_{\rm th}$. This effect becomes stronger with decreasing focusing angle because of the ever stronger self-focusing, and that leads to an apparent spot size dependence.

4) Threshold Dependence on Pulse Duration: The irradiance needed for optical breakdown with 30-ps pulses is, on average, 5.9 times higher than with 6-ns pulses, and the radiant exposure is lower by a factor of 34. The weak influence of pulse duration on $I_{\rm th}$ (and the strong influence on $F_{\rm th}$, respectively) would not be expected if cascade ionization was the only mechanism relevant for breakdown, because in that case the ionization rate would be approximately proportional to I, and a much stronger change of irradiance would be required to compensate for the shortening of pulse duration by a factor of 200. The weak influence of pulse duration on $I_{\rm th}$ indicates that multiphoton ionization with its much stronger intensity dependence must play an important role—at least for the generation of seed electrons for the ionization cascade.

The dependence between threshold radiant exposure $F_{\rm th}$ and pulse duration is, according to Koechner [35], for most solid-state laser materials given by $F_{\rm th} \propto t_L^n$, with $n = 0.5$. Our data lead to a larger value $n = 0.67 \pm 0.07$, in good agreement with the results of Zysset *et al.* [14] ($n = 0.71$) and Docchio *et al.* [11] ($n = 0.7$, averaged over the data for various spot sizes). The discrepancy between the data for distilled water and solids can be explained considering that the latter will probably have a larger impurity content than distilled water. Van Stryland *et al.* [40] observed $n = 0.5$ in NaCl and fused SiO_2 only for large focal volumes where seed electrons of an ionization cascade can be present from thermal ionization of impurities. For small focal volumes, however, they observed a stronger dependence of $F_{\rm th}$ on t_L, similar to our results. They interpret this as an indication of a multiphoton initiation of breakdown: the likelihood to find impurities within the focal volume decreases with decreasing spot size, and the medium behaves more and more like a pure substance where only multiphoton ionization can provide seed electrons. Due to the small impurity content of distilled water, it behaves like a pure medium for all spot sizes investigated.

The mean "sharpness" S of the breakdown threshold is $S = 3.55 \pm 0.77$ for 30-ps pulses, as compared to $S = 1.93 \pm 0.6$ for 6-ns pulses. The "sharper" threshold for picosecond pulses can be explained by the increasing influence of multiphoton ionization which implies a stronger dependence of the ionization rate on irradiance.

5) Threshold Dependence on Wavelength: The breakdown threshold at 532 nm for 6-ns pulses is by a factor 0.57 lower than the respective value at 1064 nm, and for 30-ps pulses it is lower by a factor of 0.83. A similar trend was observed by Kennedy *et al.* [25] for water, and by Soileau *et al.* [39] for NaCl and SiO_2. The decrease of the threshold with shorter wavelength indicates that the actual breakdown threshold is not determined by the threshold I_c for avalanche breakdown, but rather by the multiphoton processes providing the seed-electrons. I_c increases with decreasing wavelength [42, eq. (2)], whereas the threshold I_m for multiphoton ionization of seed electrons decreases since fewer photons are required for ionization (this is reflected in a higher nonlinear absorption coefficient [43]). However, although the wavelength dependence observed is in the direction predicted for multiphoton-induced breakdown, it is much weaker than expected for a pure multiphoton process [39], [43]. This suggests that avalanche and multiphoton ionization are combined in such a way that the opposite wavelength dependences of both processes largely compensate each other.

6) Comparison with Threshold Calculations: The threshold I_{MP} for pure multiphoton ionization calculated using (3) is 2.3×10^{12} W/cm^2 for 6-ns pulses, and 5.7×10^{12} W/cm^2 for 30-ps pulses at 1064 nm. These values are by a factor of 31 and 13 higher than the mean measured breakdown thresholds $I_{\rm th}$ at the respective pulse durations. This indicates that nanosecond and picosecond breakdown is not possible by pure multiphoton ionization, but dominated by cascade ionization. Multiphoton ionization is, however, needed for the initiation of the process. Table IV shows $I_{\rm th}$ in comparison to the thresholds I_m for the creation of seed electrons by multiphoton ionization and I_c for the completion of the ionization cascade. The calculations were performed using Kennedy's assumptions listed in Section II-A. For both pulse durations we find that $I_{\rm th}$ is close to I_m, especially at large focusing angles, but much larger than I_c. The breakdown threshold is thus determined by the irradiance I_m required to generate seed electrons for avalanche ionization, and not by the irradiance required for the avalanche itself which is considerably less. Since $I_{\rm th} > I_c$, the electron density at the end of the laser pulse exceeds the critical density $\rho_{\rm cr} = 10^{20}/{\rm cm}^3$ which would be reached when $I = I_c$. The ratio $I_{\rm th}/I_c$ is much larger for nanosecond pulses than for picosecond pulses. This indicates that the final electron density generated with the longer pulses must be considerably higher than with the shorter pulses. The higher electron density results in a higher absorption coefficient of the plasma [18], a stronger plasma radiation [15], a higher plasma temperature [44], and stronger mechanical effects during the plasma expansion [30]. In the next section we will show, however, that the increase of the electron density beyond $\rho_{\rm cr}$ is limited by a counteracting mechanism: due to the large value of $I_{\rm th}/I_c$ nanosecond plasmas reach a greater length (and volume) than picosecond plasmas at equal β.

The I_m values in Table IV show a distinct dependence on the focusing angle θ—in contrast to the experimental observation that $I_{\rm th}$ is independent of I_m the focusing angle. The dependence of I_m on θ is due to Kennedy's assumption of a constant *number* $N_{0\rm min}$ of initial electrons starting the ionization cascade. There is little evidence for such an assumption. It will be demonstrated below that the plasma length at threshold equals the Rayleigh range, or is even larger. For small focusing angles, the dimensions of the

TABLE IV
COMPARISON OF MEASURED BREAKDOWN THRESHOLDS $I_{\rm th}$ AT 1064 nm WITH THE VALUES I_m AND I_c CALCULATED USING (1) AND (2)

6 ns				30 ps			
$\frac{\Theta}{^\circ}$	$\frac{I_{th}}{10^{11}\,\mathrm{Wcm^{-2}}}$	$\frac{I_c}{10^{11}\,\mathrm{Wcm^{-2}}}$	$\frac{I_m}{10^{11}\,\mathrm{Wcm^{-2}}}$	$\frac{\Theta}{^\circ}$	$\frac{I_{th}}{10^{11}\,\mathrm{Wcm^{-2}}}$	$\frac{I_c}{10^{11}\,\mathrm{Wcm^{-2}}}$	$\frac{I_m}{10^{11}\,\mathrm{Wcm^{-2}}}$
32.0	0.66	0.017	1.02	28.0	4.61	0.79	4.01
22.0	0.51	0.017	0.80	22.0	4.53	0.79	3.94
8.0	0.79	0.017	0.61	14.0	6.31	0.82	3.44
5.4	1.08	0.017	0.52	8.5	4.53	0.89	2.46
1.8	0.75	0.018	0.24	4.0	3.70	0.99	1.53
				1.7	3.32	1.07	1.07

TABLE V
INITIAL ELECTRON DENSITY $\rho_{0\,\rm min}$ AND NUMBER OF SEED ELECTRONS $N_{0\,\rm min}$ FOR WHICH THE CALCULATED THRESHOLD I_m EQUALS THE MEASURED BREAKDOWN THRESHOLD $I_{\rm th}$ AT 1064 nm

6 ns			30 ps		
$\frac{\Theta}{^\circ}$	$\frac{\rho_{0min}}{10^{9}\mathrm{cm^{-3}}}$	N_{0min}	$\frac{\Theta}{^\circ}$	$\frac{\rho_{0min}}{10^{10}\mathrm{cm^{-3}}}$	N_{0min}
32.0	0.77	0.37	28.0	8.91	23
22.0	0.16	0.32	22.0	8.02	23
8.0	2.26	23	14.0	58.59	384
5.4	14.78	387	8.5	8.02	394
1.8	1.66	5010	4.0	2.38	2012
			1.7	1.24	37414
mean:	3.9		mean:	14.5	

TABLE VI
COMPARISON OF MEASURED BREAKDOWN THRESHOLDS $I_{\rm th}$ AT 532 nm AND $\Theta = 22^\circ$ WITH THE VALUES I_m AND I_c CALCULATED USING (1) AND (2), AND WITH I_{mc}

Pulse duration	$\frac{I_{th}}{10^{11}\,\mathrm{Wcm^{-2}}}$	$\frac{I_c}{10^{11}\,\mathrm{Wcm^{-2}}}$	$\frac{I_m}{10^{11}\,\mathrm{Wcm^{-2}}}$	$\frac{I_{mc}}{10^{11}\,\mathrm{Wcm^{-2}}}$
6 ns	0.29	0.0647	0.0022	0.059
30 ps	3.75	2.52	0.0506	1.37

focus are so large that the ionization cascade has to start at many independent sites to be completed within the entire focal volume during the duration of the laser pulse. It seems therefore more reasonable to assume a constant initial *density* $\rho_{0\,\rm min}$ of free electrons. To estimate $\rho_{0\,\rm min}$, we calculated the electron density [using (1)] and the number of electrons in the focal volume, for which I_m equals the measured threshold $I_{\rm th}$. For 30-ps pulses, we assumed like Kennedy that the time for the generation of the initial electrons by multiphoton ionization is $t_L/10$. For 6-ns pulses, however, we set $\Delta t = t_L/2$, because we observed that near threshold the transmission through the laser focus is markedly reduced only after the peak intensity of the laser pulse has been almost reached [18]. Table V shows the results of the calculations. The number of $N_{0\,\rm min}$ initial electrons varies by almost four orders of magnitude. For nanosecond pulses and large focusing angles, we obtained values $N_{0\,\rm min} < 1$. This is physically not possible, but the deviations from $N_{0\,\rm min} = 1$ are within the error margins given by the uncertainty of $I_{\rm th}$. The main result of the calculation is that the initial electron density $\rho_{0\,\rm min}$ created by multiphoton ionization was approximately constant (with fluctuations of one order of magnitude) for all focusing angles at both pulse durations. The average values of $\rho_{0\,\rm min}$ are 3.9×10^9 cm^{-3} for 6-ns pulses, and 14.5×10^{10} cm^{-3} for 30-ps pulses. The newly defined initial condition of $\rho_{0\,\rm min} =$ constant requires recalculation of I_c. The new I_c-values differ by less than 1% from the data given in Table IV. The ratio $I_m/I_c = I_{\rm th}/I_c$, however, has now lost its dependence on the focusing angle. The average value is 45.1 ± 13.5 for the nanosecond pulses, and 6.35 ± 1.7 for the picosecond pulses.

Kennedy *et al.* [25] found a misleading agreement between their results based on an unrealistic assumption ($N_{0\,\rm min} =$ const) and Docchio's [11] data showing an apparent spot size dependence of the breakdown threshold. Our investigations demonstrate that the spot size dependence in Docchio's study is most likely due to self-focusing effects, and that a constant density of seed electrons is a more valid assumption for the threshold calculations.

For 532 nm, we found that $I_m < I_c$ (Table VI). In this case, the actual threshold should be some intermediate value between I_m and I_c. This value can be found by incrementally increasing the initial electron density ρ_0 for the ionization cascade. As ρ_0 is increased the multiphoton initiation threshold will go up and the cascade breakdown threshold will go down, until at some value ρ_{mc} they become equal [9]. We denote the calculated threshold by I_{mc} to emphasize that both multiphoton ionization and cascade ionization contribute substantially to plasma formation. In the simplifying framework of the model, this case appears as a "jump start" for the electron avalanche. In reality, however, both mechanisms play a role throughout the whole duration of the laser pulse. We obtain $I_{mc} = 0.59 \times 10^{10}$ W·cm^{-2} for 6-ns pulses ($I_{\rm th} = 2.9 \times 10^{10}$ W·cm^{-2}), and $I_{mc} = 1.37 \times 10^{11}$ W·cm^{-2} for 30-ps pulses ($I_{\rm th} = 3.75 \times 10^{11}$ W·cm^{-2}). The agreement between calculated and measured threshold values is not as good as for 1064 nm, but still reasonable.

It is interesting to note, that the breakdown mechanisms are different at 1064 nm and at 532 nm. In the visible range, multiphoton ionization plays a larger role than in the infrared, and even at 6-ns pulse duration it yields a larger contribution than just providing seed electrons for avalanche ionization. The change of breakdown mechanisms with decreasing wavelength is probably the reason for the fact that there is hardly any wavelength dependence of the breakdown threshold: the opposite wavelength dependences of both mechanisms counterbalance each other.

The existence of two thresholds I_m and I_c for the start and the completion of the breakdown process in pure media has consequences for the breakdown-statistics. In previous

work [11], [19], [45], the probabilistic nature of optical breakdown was attributed to the statistics of avalanche ionization. In cases where $I_m > I_c$, however, it is rather due to the statistics of the multiphoton processes, because the avalanche will surely be completed once the initial electrons have been produced. If $I_m < I_c$, but $I_{\rm th} \ll I_{MP}$, the avalanche ionization process might dominate the breakdown statistics, even though more free electrons are produced by multiphoton ionization than in the first case. For $I_{\rm th} = I_{MP}$, i.e., at ultrashort pulse durations, the statistics of multiphoton ionization will take over again [46].

B. Optical Breakdown at Superthreshold Irradiance

1) Plasma Form: Fig. 5 shows the plasma form at various pulse energies for 30-ps pulses and 6-ns pulses at a constant focusing angle (22°), and Fig. 6 shows the plasma form at various focusing angles for both pulse durations at constant pulse energy (3 mJ). Plasma is created in the cone angle of the laser beam proximal to the laser. The region beyond the laser focus is "shielded" by the absorption of the laser light in the plasma. The form of the plasmas created by nanosecond- and picosecond pulses differs, probably due to the different beam profiles (see Fig. 2). Nanosecond plasmas fill the complete cone angle of the laser beam up to a long distance from the beam waist, because there is a ring of high intensity in the outer part of the beam profile. The form of picosecond plasmas follows the cone angle only near the beam waist [see, for example, Fig. 6(b), $\theta = 28°$], but becomes narrower proximal to the laser. The beam profile of the picosecond pulses is Gaussian, and at a certain distance from the beam waist the threshold irradiance $I_{\rm th}$ is therefore surpassed only near the optical axis. Apparently the plasma form approximately corresponds to lines of equal intensity bordering the region where the breakdown threshold $I_{\rm th}$ has been surpassed This is one indication for the validity of the moving breakdown model which assumes that plasma is formed at every location where $I_{\rm th}$ is exceeded.

2) Plasma Front Velocity: Another criterion for the validity of the moving breakdown model is the velocity of the plasma front during the growth of the plasma toward the incoming laser beam. The average velocity of the plasma front is given by the ratio of plasma length and pulse duration: $\overline{v} = z_{\max}/t_L$. Table VII demonstrates that $\overline{v}$ varies between 12 km/s and 76 000 km/s, depending on the focusing angle, pulse duration, and normalized pulse energy β. The peak velocities achieved in the early phase of plasma formation are even considerably higher than these average values [10]. It was already mentioned in Section II-B that a radiation-supported detonation wave [28], [29] cannot explain such high plasma front velocities, because the speed of the shock front (up to 4.5 km/s [30] is much slower than the movement of the location where the optical breakdown occurs.

3) Plasma Length: Fig. 7 shows the plasma length $z_{\max}$ as a function of laser pulse energy for various focusing angles. It is evident that there is a strong dependence of plasma length on the focusing angle. This dependence is even more pronounced for the picosecond pulses than for the nanosecond pulses. At equal energy E, picosecond plasmas are always longer than nanosecond plasmas because of the lower breakdown threshold. For a comparison of the measurement data with the moving breakdown model, the plasma length is plotted in Fig. 8 as a function of $(\beta - 1)$ on a double logarithmic scale. If (4) is valid, one should be able to fit the data by straight lines with a slope of 0.5. This is indeed possible for the 30-ps pulses [Fig. 8(a)]. All data agree within ±30%

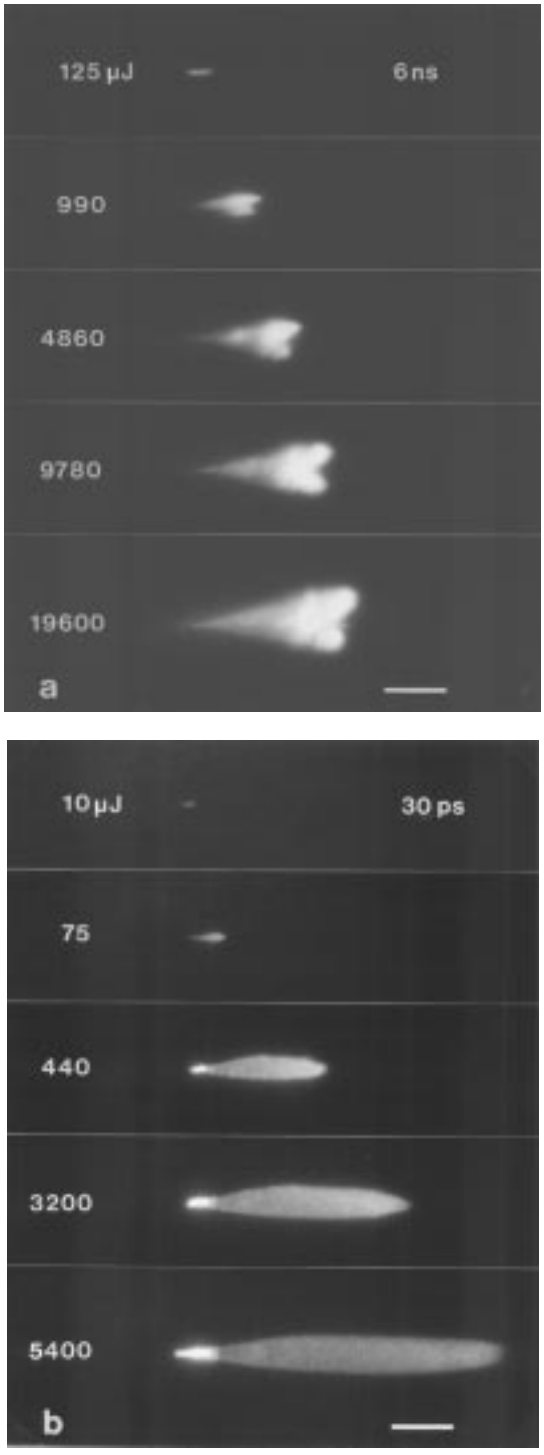

Fig. 5. Plasma form at various pulse energies. (a) 6-ns pulse duration, 22° focusing angle. (b) 30-ps pulse duration, 22° focusing angle. The values of the pulse energy are indicated on each frame. The light is incident from the right. The bar represents a length of 100 μm.

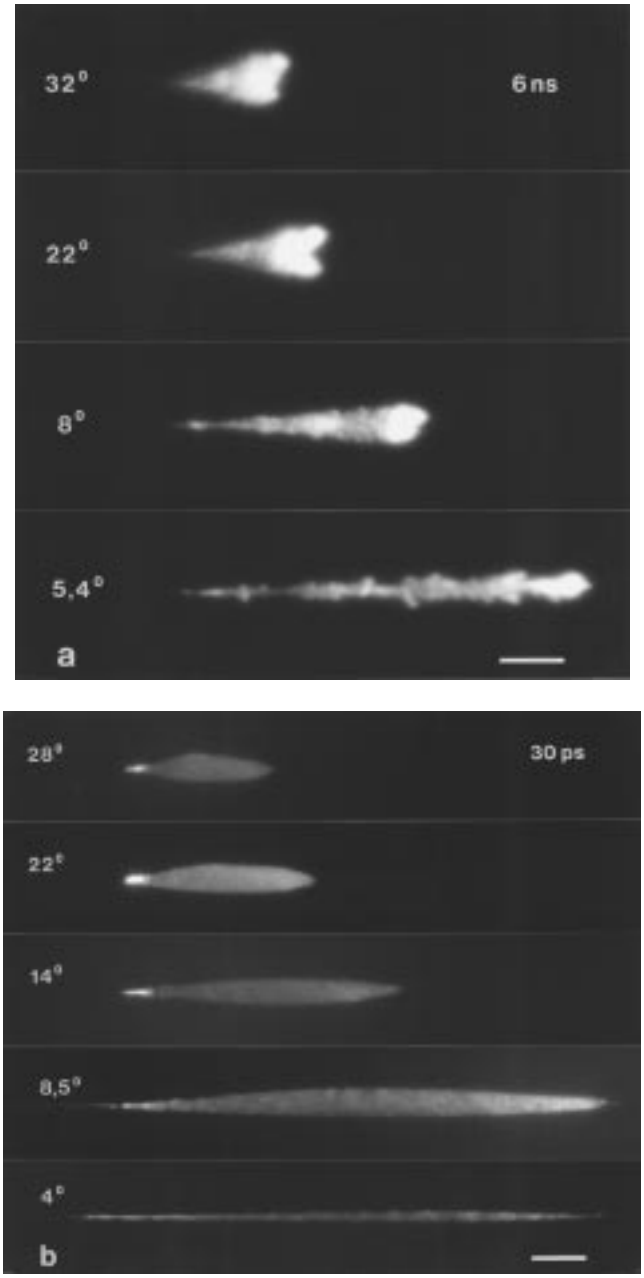

Fig. 6. Plasma form at various focusing angles. (a) 6-ns pulse duration, 10-mJ pulse energy. (b) 30-ps pulse duration, 3-mJ pulse energy. The focusing angles are indicated on each frame. The light is incident from the right. The bar represents a length of 100 μm.

TABLE VII
AVERAGE PLASMA FRONT VELOCITY FOR VARIOUS FOCUSING ANGLES AND NORMALIZED PULSE ENERGIES β

6 ns			30 ps		
	$\beta = 10$	$\beta = 100$		$\beta = 100$	$\beta = 1000$
$\frac{\Theta}{°}$	$\frac{v}{\mathrm{km\,s^{-1}}}$	$\frac{v}{\mathrm{km\,s^{-1}}}$	$\frac{\Theta}{°}$	$\frac{v}{\mathrm{km\,s^{-1}}}$	$\frac{v}{\mathrm{km\,s^{-1}}}$
32.0	12.5	23.3	28.0	2500	8670
22.0	16.7	38.3	22.0	3330	11300
8.6	48.3		14.0	7330	26300
8.0	50.0		8.5	19000	
5.4	133.3		4.0	76000	

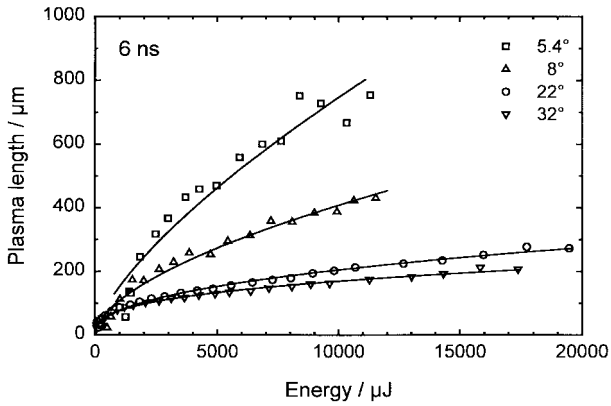

(a)

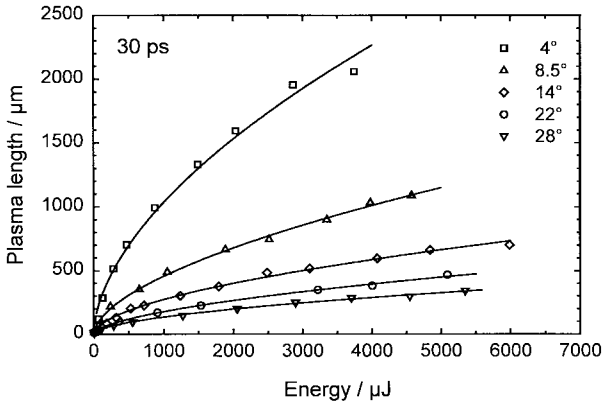

(b)

Fig. 7. Plasma length $z_{\max}$ as a function of laser pulse energy for various focusing angles. (a) 6-ns pulse duration. (b) 30-ps pulse duration.

with the values predicted by (4), and the $z_{\max}(\theta)$-dependence follows (5). The agreement is not as good for the nanosecond pulses [Fig. 8(b)], neither with respect to the slope which varies between 0.31 and 0.47, nor with respect to the absolute values for the plasma length and the $z_{\max}(\theta)$-dependence. According to the model, nanosecond plasmas should have the same length as picosecond plasmas at equal β, but in fact they are considerably longer (Fig. 9). At $\beta = 10°$ and $\beta = 22°$, for example, the nanosecond plasma is 100 μm long, whereas the picosecond plasma measures only 25 μm (the model predicts $z_{\max} = 27$ μm). The relative deviation of nanosecond plasmas from the predicted plasma length is strongest for large focusing angles and near the breakdown threshold.

The deviation from the model is probably partly due to the UV-radiation emitted by plasma produced early during the laser pulse. The radiation provides initial electrons for ionization cascades occurring in the vicinity of the plasma [47]. Once plasma is formed, the breakdown process is thus independent of the creation of initial electrons by multiphoton ionization, and the threshold is lowered from I_m to a value closer to I_c. Due to the reduction of I_{th} during the laser pulse, the plasma grows further than predicted by the moving breakdown model which assumes a constant threshold. The situation is different in picosecond breakdown where I_m is

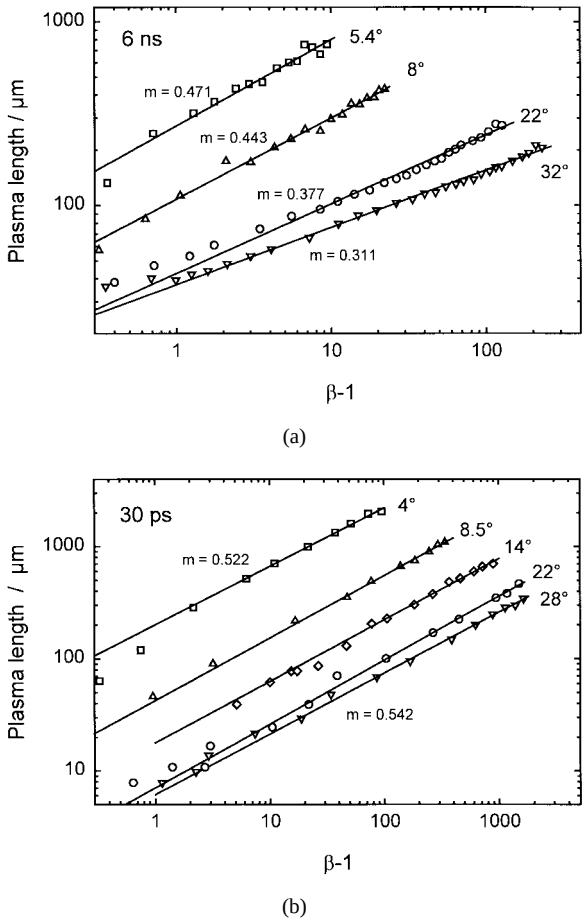

Fig. 8. Plasma length $z_{\max}$ as a function of $(\beta - 1)$ for various focusing angles. (a) 6-ns pulse duration. (b) 30-ps pulse duration. Docchio's moving breakdown model predicts straight lines with a slope of 0.5.

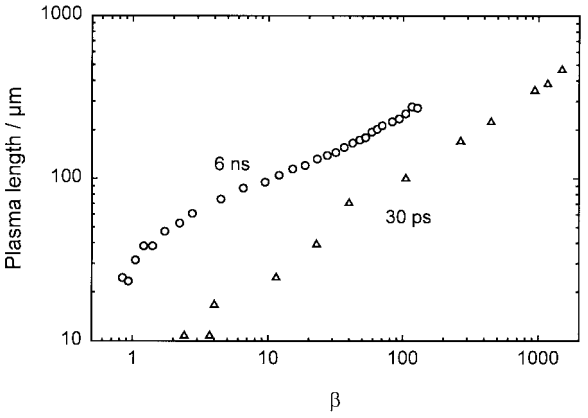

Fig. 9. Comparison of the plasma length observed with 6-ns and 30-ps pulse duration plotted as a function of β. The focusing angle is 22°. Docchio's moving breakdown model predicts that at equal β the plasma length is independent of pulse duration.

anyway closer to I_c. Therefore, the picosecond threshold is much less influenced by the plasma radiation and remains approximately constant during the breakdown process, as assumed by the model. Wavelength and penetration depth of the plasma radiation are compatible with the above interpretation. Spectroscopic analysis of the radiation from plasmas produced in distilled water led to estimates for the plasma temperature of about 10 000 K [44] and 15 000 K [22] for nanosecond pulses, and of 6200 K [44] for picosecond pulses. Blackbody radiation at these temperatures contains wavelengths below 200 nm. Grand *et al.* [24] determined values of 6.5–7.0 eV for the ionization potential and energy gap of pure liquid water considered as a semiconductor. This energy range corresponds to a wavelength range between 177 nm and 190 nm, and a penetration depth $d = 1/\alpha$ between 110 μm (at 177 nm) and 4 cm (at 191 nm) [23]. The penetration depth of the UV-photons is thus large enough to explain the deviation of the plasma length from the moving breakdown model observed with nanosecond pulses which, depending on focusing angle and pulse energy, is between 30 μm and 800 μm.

A second reason for the discrepancy between model predictions and experimental data is that the model in its present form does not account for aberrations of the laser beam. We performed all calculations of the plasma length using the diffraction limited spot size corresponding to the focusing angle measured at large distances from the beam waist. This is a good approach for large β-values where the Gaussian $\omega(z)$-curve is similar to the actual shape of $\omega(z)$. Near threshold, however, plasma is formed only in the region of the beam waist which is deformed when aberrations are present. If the measured spot size is, for example, two times larger than the diffraction limited spot, the corresponding Rayleigh range $z_R = \pi\omega_0^2/\lambda$ is four times larger, and the plasma length will increase accordingly. In our experiments, aberrations were stronger for nanosecond pulses than for picosecond pulses (see Tables I and II), and, therefore, nanosecond plasmas tend to be larger, especially near threshold and at large focusing angles where the influence of aberrations is most pronounced.

4) Inhomogeneities Within the Plasma: In general, both picosecond and nanosecond plasmas are fairly homogeneous (Figs. 5 and 6), and we did not observe multiple plasma formation as reported by other authors [13], [48]. This is due to the use of distilled and filtered water, and to the minimization of optical aberrations which eliminates "hot spots" in the focal region of the laser beam [41]. The free electrons produced by UV-radiation emitted from plasma created early during the laser pulse may further contribute to the formation of homogeneous plasmas, especially for nanosecond pulses, where the generation of seed electrons is the limiting factor for plasma formation. Due to the plasma radiation, seed electrons are always present, and optical breakdown in the vicinity of earlier produced plasma largely looses its statistical character. Only at a small focusing angle of 5.4°, the borderline of the nanosecond plasmas is not smooth any more [Fig. 6(a)]. Here, the penetration depth of the UV-radiation or its intensity may be too small, with respect to large plasma front velocity, to guarantee a homogeneous plasma structure.

At irradiances far above the breakdown threshold, picosecond plasmas exhibit a bright spot near the beam waist [Figs. 5(b) and 6(b)]. The threshold irradiance leading to the formation of the bright spot can be calculated using the

plasma transmission data from Part II of our paper [18]. Assuming, for the sake of simplicity, that the transmission is constant throughout the laser pulse and the focal spot size is not influenced by self-focusing, we obtain a threshold value of $1.7 \pm 0.5 \times 10^{13}$ W/cm^2 for the formation of the bright spot. This irradiance is 43 times higher than the average breakdown threshold for picosecond pulses, and three times higher than the calculated threshold I_{MP} at which the critical electron density $\rho = 10^{20}/\text{cm}^3$ could be reached by pure multiphoton ionization alone. Therefore, a very high electron density in the focal region will be reached which explains the bright plasma radiation. Self-focusing effects in the plasma [49] may even further increase the irradiance in the focal region and thus the electron density reached.

With nanosecond pulses, the plasma is brightest at the side proximal to the laser. This can be explained by the high-electron density reached in the nanosecond plasmas (see Section IV-A) which leads to a high-absorption coefficient [18] and, hence a small-penetration depth of the laser light into the plasma.

V. Summary and Conclusion

We investigated the optical breakdown in water for 30-ps pulses and 6-ns pulses at threshold and superthreshold irradiances. The average threshold I_{th} for optical breakdown was by a factor of 5.9 higher for the picosecond pulses ($I_{\text{th}} = 4.5 \times 10^{11}$ W/cm^2) than for the nanosecond pulses ($I_{\text{th}} = 0.76 \times 10^{11}$ W/cm^2), and the mean radiant exposure threshold F_{th} was by a factor of 34 higher for the nanosecond pulses (453 J cm^{-2}) than for the picosecond pulses (13.5 J cm^{-2}). We found no systematic spot size dependence of the breakdown threshold in the range investigated between 5- and 50-μm spot diameter. An apparent spot size dependence arises, however, when the thresholds are calculated using diffraction limited spot sizes neglecting optical aberrations and self-focusing effects. Aberrations play a role mainly at large focusing angles, and self-focusing effects influence the breakdown threshold at focusing angles below approximately 2°.

The experimental data were analyzed using Kennedy's model for the calculation of breakdown thresholds [9]. For both pulse durations and a wavelength of 1064 nm the measured thresholds I_{th} are approximately equal to the calculated threshold I_m for the generation of seed electrons by multiphoton ionization, and are considerably higher than the irradiance I_c for the completion of the ionization cascade during the laser pulse. Optical breakdown in distilled water with pulses of 30-ps and 6-ns duration is therefore due to cascade ionization initiated by multiphoton ionization. An initial electron density of about 4×10^9 cm^{-3} is required to start of the ionization avalanche with 6-ns pulses, and a density of 1.4×10^{11} cm^{-3} is necessary with 30-ps pulses, regardless of the focal spot size. At 532 nm, multiphoton ionization does not only provide seed electrons for the avalanche process, but contributes considerably to the creation of free electrons throughout the whole process of plasma formation. The breakdown statistics at both wavelengths are therefore strongly influenced by multiphoton processes and cannot be described considering only the probabilistic nature of the avalanche process. The exponential dependence of the multiphoton ionization rate on irradiance explains the weak dependence of the irradiance threshold on laser pulse duration. Nanosecond pulses create a higher electron density at the end of the laser pulse than picosecond pulses. The higher electron density results in a higher absorption coefficient of the plasma, a stronger plasma radiation, a higher plasma temperature, and stronger mechanical effects.

Plasma formation at superthreshold energies cannot be explained by a radiation-supported detonation wave, but only by a "breakdown wave" mechanism. The plasma length $z_{\max}$ reached during the laser pulse depends strongly on the focusing angle, whereby this dependence is more pronounced for the picosecond pulses than for the nanosecond pulses. The dependence of plasma length on the normalized laser pulse energy β can be expressed by $z_{\max} \propto (\beta - 1)^n$ with $n = 0.54 \pm 0.02$ for picosecond pulses, and $0.31 \leq n \leq 0.47$ for nanosecond pulses. At equal pulse energy E, nanosecond plasmas are always shorter than picosecond plasmas, whereas at equal β, nanosecond plasmas are always longer. Docchio's moving breakdown model [10] which assumes a time-invariant breakdown threshold, gives an adequate description of the plasma length for picosecond pulses, both for the absolute values of the plasma length, and for the $z_{\max}(\beta)$ dependence. It underestimates, however, the length of the plasmas produced by nanosecond pulses. The disagreement between the experimentally determined plasma length and the model predictions can partly be explained by a decrease of the breakdown-threshold during the nanosecond pulses caused by the UV-part of the plasma-radiation. A further reason for the disagreement are deformations of the beam waist by aberrations which are not accounted for in the present form of the model.

Clinical Consequences

In plasma-mediated intraocular laser surgery, the primary effect of the laser pulses consists of the evaporation of the tissue within the plasma volume [4]. A higher surgical precision can be achieved with picosecond pulses than with nanosecond pulses [34], because picosecond pulses have a lower energy threshold for optical breakdown, and the size of picosecond plasmas near threshold is smaller than that of nanosecond plasmas. The data presented in this paper can serve as basis to infer the plasma length as a function of pulse energy and focusing angle. At equal energy, picosecond pulses create larger plasmas and thus evaporate more tissue. In [15] and [30], it is shown that this goes along with a smaller percentage of energy transformed into mechanical energy. Picosecond pulses are therefore advantageous where precise cutting with little disruptive side effects is required. In applications as posterior capsulotomy [3], however, where photodisruptive capsule tearing is a desirable part of the surgical effect, nanosecond pulses may be better suited because of their stronger mechanical action.

ACKNOWLEDGMENT

The authors thank S. Rein for his contribution in the early phase of the project, and appreciate helpful discussions with F. Docchio, P. Kennedy, B. Rockwell, and R. Birngruber.

REFERENCES

[1] S. J. Gitomer and R. D. Jones, "Laser-produced plasmas in medicine," *IEEE Trans. Plasma Sci.*, vol. 19, pp. 1209–1219, 1991.
[2] A. Vogel, "Nonlinear absorption: Intraocular microsurgery and laser lithotripsy," *Phys. Med. Biol.*, vol. 42, pp. 1–18, 1996.
[3] R. F. Steinert and C. A. Puliafito, The *Nd : YAG Laser in Ophthalmology*. Philadelphia, PA: Saunders, 1985.
[4] A. Vogel, P. Schweiger, A. Frieser, M. Asiyo, and R. Birngruber, "Intraocular Nd : YAG laser surgery: Light-tissue interaction, damage range, and reduction of collateral effects," *IEEE J. Quantum Electron.*, vol. 26, pp. 2240–2260, 1990.
[5] N. Bloembergen, "Laser-induced electric breakdown in solids," *IEEE J. Quantum Electron.* vol. QE-10, pp. 375–386, 1974.
[6] C. G. Morgan, "Laser-induced breakdown in gases," *Rep. Prog. Phys.* vol. 38, pp. 621–665, 1975.
[7] D. C. Smith and R. G. Meyerand, "Laser radiation induced gas breakdown," in *Principles of Laser Plasma*, G. Bekefi, Ed. New York: Wiley, 1976, pp. 457–507.
[8] G. M. Weyl, "Physics of laser-induced breakdown: An update," in *Laser-Induced Plasmas and Applications*, L. J. Radziemski and D. A. Cremers, Eds. New York: Marcel Dekker, 1989, pp. 1–67.
[9] P. K. Kennedy, "A first-order model for computation of laser-induced breakdown thresholds in ocular and aqueous media Part I—Theory," *IEEE J. Quantum Electron.*, vol. 31, pp. 2241–2249, 1995.
[10] F. Docchio, P. Regondi, M. R. C. Capon, and J. Mellerio, "Study of the temporal and spatial dynamics of plasmas induced in liquids by nanosecond Nd : YAG laser pulses 1—Analysis of the plasma starting times," *Appl. Opt.*, vol. 27, pp. 3661–3668, 1988.
[11] F. Docchio, C. A. Sacchi, and J. Marshall, "Experimental investigation of optical breakdown thresholds in ocular media under single pulse irradiation with different pulse durations," *Lasers Ophthalmol.*, vol. 1, pp. 83–93, 1986.
[12] C. A. Sacchi, "Laser-induced electric breakdown in water," *J. Opt. Soc. Amer. B*, vol. 8, pp. 337–345, 1991.
[13] H. P. Loertscher, "Laser-induced breakdown for ophthalmic applications," in *YAG Laser Ophthalmic Microsurgery*, S. C. Trokel, Ed. Norwalk, CT: Appleton-Century-Crofts, 1983, pp. 39–66.
[14] B. Zysset, J. G. Fujimoto, and T. F. Deutsch, "Time-resolved measurements of picosecond optical breakdown," *Appl. Phys. B*, vol. 48, pp. 139–147, 1989.
[15] A. Vogel, S. Busch, K. Jungnickel, and R. Birngruber, "Mechanisms of intraocular photo disruption with picosecond and nonosecond laser pulses," *Lasers Surg. Med.*, vol. 15, pp. 32–43, 1994.
[16] M. M. T. Loy and Y. R. Shen, "Study of self-focusing and small-scale filaments of light," *IEEE J. Quantum Electron.*, vol. QE-9, pp. 409–422, 1973.
[17] W. L. Smith, P. Liu, and N. Bloembergen," Superbroadening in H_2O and D_2O by self-focused picosecond pulses from a YAlG : Nd laser," *Phys. Rev. A*, vol. 15, pp. 2396–2403, 1977.
[18] K. Nahen and A. Vogel, "Plasma formation in water by picosecond and nanosecond Nd:YAG laser pulses—II: Plasma transmission, scattering, and reflection," this issue, pp. 861–871.
[19] F. Docchio, L. Dossi, and C. A. Sacchi, "Q-switched Nd : YAG laser irradiation of the eye and related phenomena: An experimental study I—Optical breakdown determination for liquids and membranes," *Lasers Life Sci.*, vol. 1, pp. 87–103, 1986.
[20] Yu. P. Raizer, "Breakdown and heating of gases under the influence of a laser beam," *Sov. Phys.—Usp.*, vol. 8, pp. 650–673, 1966.
[21] M. Bass and H. H. Barrett "Avalanche breakdown and the probabilistic nature of laser-induced damage," *IEEE J. Quantum Electron.*, vol. QE-8, pp. 338–343, 1972.
[22] P. A. Barnes and K. E. Rieckhoff, "Laser induced underwater sparks," *Appl. Phys. Lett.*, vol. 13, pp. 282–284, 1968.
[23] F. Williams, S. P. Varama, and S. Hillenius, "Liquid water as a lone-pair amorphous semiconductor," *J. Chem. Phys.*, vol. 64 pp. 1549–1554, 1976.
[24] D. Grand, A. Bernas, and E. Amouyal, "Photoionization of aqueous indole; conducting band edge and energy gap in liquid water," *Chem. Phys.*, vol. 44, pp. 73–79, 1979.
[25] P. K. Kennedy, S. A. Boppart, D. X. Hammer, B. A. Rockwell, G. D. Noojin, and W. P. Roach, "A first-order model for computation of laser-induced breakdown thresholds in ocular and aqueous media Part II—Comparison to experiment," *IEEE J. Quantum Electron.*, vol. 31, pp. 2250–2257, 1995.
[26] Y. R. Shen, *The Principles of Nonlinear Optics*, New York: Wiley, 1984, pp. 528–540.
[27] L. V. Keldysh, "Ionization in the field of a strong electromagnetic field," *Sov. Phys.—JETP*, vol. 20, pp. 1307–1314, 1965.
[28] S. A. Ramsden and P. Savic, "A radiative detonation model for the developement of a laser-induced spark in air" *Nature*, vol. 203, pp. 1217–1219, 1965.
[29] J. W. Daiber and H. M. Thompson, "Laser-driven detonation waves in gases," *Phys. Fluids*, vol. 10, pp. 1162–1169, 1967.
[30] A. Vogel and S. Busch, "Shock wave emission and cavitation bubble generation by picosecond and nanosecond optical breakdown in water," *J. Acoust. Soc. Amer.*, vol. 100, pp. 148–165, 1996.
[31] G. E. Duvall and G. R. Fowles, "Shock waves," in *High Pressure Physics and Chemistry*, R. S. Bradley, Ed. New York: Academic, 1963, pp. 209–291.
[32] R. V. Ambartsumyan, N. G. Basov, V. A. Boiko, V. S. Zuev, O. N. Krokhin, P. G. Kryukov, Yu. V. Senatskii, and Yu. Yu. Stoilov, "Heating of matter by focused laser radiation," *Sov. Phys.—JETP*, vol. 21, pp. 1061–1064, 1965.
[33] V. Magni, S. DeSilvestri, and A. Cybo-ottone, "Resonators with variable reflectivity mirrors," in *The Physics and Technology of Laser Resonators*, D. R. Hall and P. E. Jackson, Eds. New York: Adam Hilger, 1989, pp. 94–105.
[34] A. Vogel, M. R. C. Capon, M. N. Asiyo, and R. Birngruber, "Intraocular photodisruption with picosecond and nanosecond laser pulses: Tissue effects in cornea, lens and retina," *Invest. Ophtalmol. Vis. Sci.*, vol. 35, pp. 3033–3044, 1994.
[35] W. Koechner, *Solid State Laser Engineering*. Berlin, Germany: Springer, 1988.
[36] A. E. Siegman, M. W. Sasnett, and T. F. Johnston, "Choice of clip levels for beam width measurements using knife-edge techniques," *IEEE J. Quantum Electron.*, vol. 27, pp. 1098–1104, 1991.
[37] N. W. Sasnett, "Propagation of multimode laser beams—the M^2 factor," in *The Physics and Technology of Laser Resonators*, D. R. Hall and P. E. Jackson, Eds.New York: Adam Hilger, 1989, pp. 94–105.
[38] J. H. Marburger, "Self-focusing: Theory" in *Progress Quantum Electron.*, vol. 4. Oxford, U.K.: Pergamon, 1975, pp. 35–110.
[39] M. J. Soileau, W. F. Williams, N. Mansour, and E. W. Van Stryland, "Laser-induced damage and the role of self-focusing," *Opt. Eng*. vol. 28, pp. 1133–1144, 1989.
[40] E. W. Van Stryland, M. J. Soileau, A. L. Smirl, and W. E. Williams, "Pulsewidth and focal-volume dependence of laser-induced breakdown," *Phys. Rev. B*, vol. 23, pp. 2144–2151, 1981.
[41] L. R. Evans and C. Grey Morgan, "Lens aberration effects in optical-frequency breakdown of gases," *Phys. Rev. Lett.*, vol. 22, pp. 1099–1102, 1969.
[42] M. Sparks, D. L. Mills, R. Warren, T. Holstein, A. A. Maradudin, L. J. Sham, E. Loh, and D. F. King, "Theory of electron-avalanche breakdown in solids," *Phys. Rev. B*, vol. 24, pp. 3519–3536, 1981.
[43] B. S. Wherret, "Scaling rules for multiphoton interband absorption in semiconductors," *J. Opt. Soc. Amer. B*, vol. 1, pp. 67–72, 1984.
[44] D. J. Stolarski, J. Hardman, C. G. Bramlette, G. D. Noojin, R. J. Thomas, B. A. Rockwell, and W. P. Roach, "Integrated light spectroscopy of laser-induced breakdown in aqueous media," *SPIE Proc.*, vol. 2391, pp. 100–109, 1995.
[45] H. Schmidt-Kloiber, G. Paltauf, and E. Reichel, "Investigation of the probabilistic behavior of laser-induced breakdown in pure water and in aqueous solutions of different concentrations," *J. Appl. Phys.*, vol. 66, pp. 4149–4153, 1989.
[46] D. X. Hammer, R. J. Thomas, G. D. Noojin, B. A. Rockwell, P. K. Kennedy, and W. P. Roach, "Experimental investigation of ultrashort pulse laser-induced breakdown thresholds in aquesous media," *IEEE J. Quantum Electr*. vol. 32, pp. 670–678, 1996.
[47] A. J. Alcock, C. DeMichelis, K. Hamal, and B.A. Tozer, "Expansion mechanism in a laser-produced spark," *Phys. Rev. Lett.*, vol. 20, pp. 1095–1097, 1968.
[48] M. R. C. Capon, F. Docchio, and J. Mellerio, "Investigations of multiple plasmas from ophthalmic Nd : YAG lasers," *Lasers Ophthalmol.* vol. 1, pp. 95–106, 1986.
[49] R.H. Hora, H.G.L. Coster, C.J. Walter, and H. Hora, "Self-focusing limits at the laser-plasma interaction for treatment of cataract with nanosecond and picosecond pulses," *Laser Part. Beams*, vol. 10, pp. 163–178, 1992.

Alfred Vogel studied physics and sociology at the Georg-August University of Göttingen, Germany, where he received the Ph.D. degree in physics in 1987.

From 1988–1992 he was a Research Member of the laser laboratory at the University Eye Hospital in Munich, and since 1992 he is a Senior Scientist at the Medical Laser Center Lübeck. He was a Chairman of the Gordon Research Conference on Laser Applications in Medicine and Biology in 1996. His research interests include laser tissue interactions in photodisruption, pulsed laser ablation, and photocoagulation, as well as laser-induced plasma formation, cavitation, and shock waves.

Dr. Vogel is a Member of the German Physical Society, the Optical Society of America, the Acoustical Society of America, and the Association for Research in Vision and Ophthalmology.

Kester Nahen studied physics at the University of Hamburg, Germany, from 1990 to 1996. He received the diploma degree from the Medical Laser Center Lübeck, Germany. Since spring 1996, he has been persuing the Ph.D. degree in physics at the Medical University of Lübeck.

His current fields of interest include laser-induced plasma formation and pulsed laser ablation of tissues.

Mr. Nahen is a Member of the German Physical Society and of the Society of German Scientists and Physicians.

Dirk Theisen received the Diploma degree in physical engineering from the Polytechnic of Lübeck, Germany, in 1995.

Currently he is a Research Engineer at the Medical Laser Center Lübeck. His research interests include laser-induced plasma formation and laser-assisted myocardial revascularization.

Joachim Noack received the M.Sc. degree in "Optoelectronics and Laser Devices" from St. Andrews University, Scotland, U.K., in 1993. Currently he is a Research Assistant at the Medical Laser Center Lübeck, Germany, pursuing the Ph.D. degree in physics.

His major areas of interest are optical breakdown phenomena, pulsed laser ablation, ultrafast photography, and image processing for biomedical applications.

Mr. Noack is a Member of the German Physical Society.